arXiv:astro-ph/0501086v2 10 Jan 2005

Redshifted 21 cm Emission From the Pre-Reionization Era II. H II Regions Around Individual Quasars

Katharina Kohler, Nickolay Y. Gnedin
CASA, University of Colorado, Boulder, CO 80309, USA; kohlerk,gnedin@casa.colorado.edu

Jordi Miralda-Escudé
Department of Astronomy, Ohio State University, Columbus, OH 43210; jordi@astronomy.ohio-state.edu
and

Peter A. Shaver
ESO, Karl-Schwarzschild-Strasse 2, Garching, D-85748, Germany; pshaver@eso.org

ABSTRACT

We use cosmological simulations of reionization to predict the effect of large H II regions around individual high-redshift quasars on the possible signal from the redshifted 21 cm line of neutral hydrogen in the pre-reionization era. We show that these H II regions appear as "spectral dips" in frequency space with equivalent widths in excess of 3 mK MHz or depths in excess of about 1.5 mK, and that they are by far the most prominent cosmological signals in the redshifted H I distribution.

These spectral dips are expected to be present in almost every line of sight. If the spectral dips of a large enough sample of H II regions are well resolved in frequency space, the distribution of line depth and equivalent width in frequency with a known observing beamsize can be used to infer the H II region size distribution and the mean difference in neutral hydrogen density between the H II regions (which may contain self-shielded neutral gas clumps) and the surrounding medium, providing a powerful test for models of reionization.

Subject headings: cosmology: theory - cosmology: large-scale structure of universe - diffuse radiation - galaxies: formation - galaxies: intergalactic medium - radio lines: general

1. Introduction

Theoretical interest in the redshifted 21 cm line signal from intergalactic hydrogen before and during the reionization era has surged in recent years. Fluctuations in the 21 cm signal can be generated by variations in the density, spin temperature, or ionized fraction of the intergalactic gas. These could arise from primordial density fluctuations, from spatial variations of the radiation intensity near the wavelength of the Ly-α hydrogen line (which affects the spin temperature), from other radiation that can heat the gas, or from H II regions created during the process of reionization by discrete sources. The latter source of 21 cm fluctuations was discussed in the pioneering work of Scott & Rees (1990), Madau, Meiksin, & Rees (1997), and Tozzi et al. (2000), but has received only limited attention recently (Wyithe & Loeb 2004).

However, ionized (H II) regions around high-redshift quasars can easily reach sizes comparable to the angular beams of future radio telescopes such as LOFAR and SKA. Thus, they could be the most prominent features in the angular and frequency distribution of the redshifted 21 cm signal from the early universe, and the first features

to be measured observationally.

In this paper we estimate the effects of these large features on the possible cosmological signal by using numerical simulations of reionization. This becomes feasible now as simulations of reionization reach the level of sophistication and accuracy sufficient to model quantitatively not only the small-scale details of reionization (Gnedin 2004), but also very large regions (up to a horizon size: Kohler, Gnedin, & Miralda-Escudé 2004). The latter approach is used here, because quasars are relatively rare at high redshift, and sufficiently large computational volumes (several hundred Mpc in size) must be used to include a representative sample of quasars.

We concentrate solely on the redshifted 21 cm signal in the frequency domain, because, as has been shown before, foreground contamination is a severe limiting factor in observing the cosmological features in the angular domain on the sky (Di Matteo et al. 2002; Oh & Mack 2004; Gnedin & Shaver 2004). Several recent papers have discussed elegant and sophisticated approaches to circumventing this contamination (Zaldarriaga, Furlanetto & Hernquist 2004; He et al. 2004; Santos et al. 2004, Loeb & Zaldarriaga 2004), but these approaches would require bigger telescopes than currently planned, so it is most likely that the first detections will be made in the frequency domain and attempts to de-contaminate the angular signal will require follow-on observations.

2. Simulation

In order to model the spectral signatures of H II regions in the early universe, we need to simulate a large enough region of space that includes bright quasars during the reionization era. Such quasars are sparse at high redshift, since in the hierarchical structure formation paradigm they only form in extreme over-densities at early times.

The simulation code we use is a modified version of the "Softened-Lagrangian Hydrodynamics" code described in Gnedin (2004), which follows the evolution of dark matter and gas. The code includes a model for star formation in regions of dense gas that can cool, and for the emission of ionizing radiation from stars. Radiative transfer is fully included using the method described in Gnedin & Abel (2001), and the ionization state of the gas is followed in every cell as determined by the local radiation intensity.

In this specific project we use a multi-resolution approach that utilizes a small-scale simulation as a "sub-cell" model for larger-scale simulations. The "sub-cell" model is implemented by using the so-called "clumping factors", which account for the structure on scales too small to be resolved in a large-scale simulation. The complete description of our approach and the appropriate tests are presented in a separate paper (Kohler et al. 2004).

Using the clumping factor formalism allows us to increase the size of the simulation box to several hundred comoving Mpc, while simultaneously accounting for the ionizing radiation transfer and recombination rate in a gaseous medium that is highly inhomogeneous on small scales.

In our simulation of reionization, we add individual quasars as discrete, luminous sources of ionizing radiation in addition to the emission associated with star-formation. The luminosity distribution of quasars added to the simulation is chosen from the model of Schirber & Bullock (2003). This model is consistent with all known observational data on the evolution of the quasar luminosity function, including recent GOODS data (Cristiani et al. 2004). The impact of quasars on reionization depends of course on the luminosity function at very high redshift, $z = 6$, before reionization ended, so we have to extrapolate the Schirber & Bullock model to redhifts higher than observed quasar redshifts, which introduces a substantial uncertainty. Our goal, therefore, is to discuss a range of possibilities, as precise predictions are not possible. The extrapolated luminosity function of quasars introduced in the simulation is shown in Figure 1 for $z = 10$; the finite box size causes the discreteness effects observed at high luminosity end. Our simulation box includes quasars up to a luminosity of about $10^{12} L_{Sun}$ at $z = 10$ (although quasars this luminous are rare, and therefore appear in only a few lines of sight).

In our simulation we include biasing of sources of ionizing and Ly-α radiation. Specifically, we assume that galaxies are biased with a bias factor of two, while quasars are biased with a bias factor of three. In this work we do not consider redshift-dependent bias factors.

The specific simulation used in this paper has

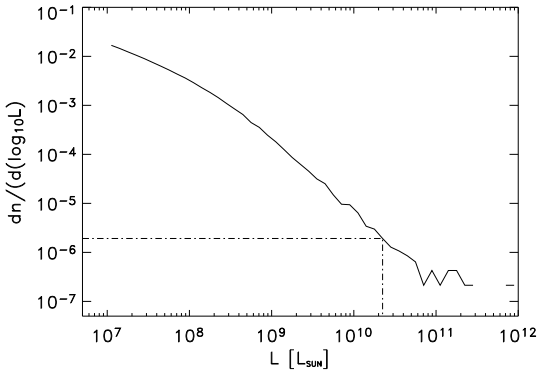

Fig. 1.— Our adopted quasar luminosity function at $z = 10$, as extrapolated from Schirber and Bullock (2003). The dash-dotted line shows the luminosity of a typical quasar which is expected to be present in almost all $10'$ observational beams.

128^3 cells with an average comoving cell size of $2h^{-1}$ Mpc. The box size of $256h^{-1}$ Mpc allows us to resolve individual H II regions around typical quasars at $z \sim 8 - 10$, although it is still too small to include the brightest high-redshift quasars found in the Sloan Digital Sky Survey (Fan et al. 2003). But since we are interested in typical (rather than the rarest, most extreme) features in the redshifted 21 cm signal, this simulation is sufficient for our purpose.

3. 21 cm "Spectral Dips" due to Quasar H II Regions

We now investigate the characteristics of H II regions as they appear in the redshifted 21 cm spectra from neutral hydrogen. The intergalactic hydrogen can be observed in absorption or emission against the CMB, depending on whether the spin temperature is lower or higher than the CMB temperature. Although an absorption signal is expected when the earliest emission of Ly-α photons occurs (which couples the spin and kinetic temperature of hydrogen, bringing the spin temperature below the CMB temperature; see Madau et al. 1997), the 21 cm signal in our simulation quickly turns into emission, as X-rays, far-ultraviolet radiation, and weak shocks from structure formation heat the atomic gas to a temperature higher than the CMB (e.g., Chen & Miralda-Escudé 2004; Gnedin & Shaver 2004). For the redshift range that we consider in this paper (corresponding to frequencies largely above the FM bands), the atomic gas is heated above the CMB temperature and produces an emission signal. Therefore, H II regions should produce dips in the spectrum because they contain less neutral hydrogen than their environment, so their emission is reduced compared to the regions around them. We shall generally refer to these H II region features as dips. Note that these dips look like absorption features even though they have nothing to do with absorption.

The basic observable properties of the spectral dip of an H II region are its width and depth. The depth depends on the ionization fraction, gas density, spin temperature, and also on the angular size of the H II region if this angular size is not resolved by the beam of the radio telescope that is used (the angular size of a typical observable H II region is about $1.5 - 2$ arcmin). The width of the spectral dip in frequency space is determined by the radial extent of the ionized region (assuming that peculiar velocities are small compared to the Hubble expansion across the H II region).

In practice, the detected cosmological H II regions will probably be smaller than the angular size of the radio beam. However, if the H II regions are resolved in frequency, their frequency width determines their size. Thus, the average linear (and angular) size for a sufficiently large sample of observed H II regions can be estimated (for a given cosmological model) from the frequency data alone, and, taking into account the dilution by the known radio beamsize, the actual average depth of the spectral dip can be inferred from the measured dip depth.

In this paper, however, we do not investigate such a measurement any further, because it will most likely require a large number of independent lines of sight.

The average depth of a spectral dip is related to the difference in the amount of neutral hydrogen present (on average) inside and outside an H II region. The observational determination of this quantity would introduce a new tool for testing models of reionization. In the H II regions the fraction of gas that is still atomic depends on how much of the gas in collapsed, low-mass halos remains self-shielded, and how much has been

ionized and evaporated from halos (e.g., Shapiro, Iliev, & Raga 2004), a process that is important to determine the clumping factors of ionized gas. Outside the identified H II regions, the fraction of gas already ionized depends on the presence of hard photons and low-luminosity sources producing unresolved ionized regions. Determining the dip depth distribution will require a large number of independent lines of sight, and the theoretical interpretation will be complex. In the rest of this paper we focus on how spectral dips due to H II regions can be identified.

In the absence of H II regions, the distribution of brightness temperature of the redshifted 21 cm signal should be Gaussian, reflecting the imprints of cosmic density fluctuations, which are linear on the large scales that are most easily observable. The H II regions add additional features in the spectrum that are mainly caused by variations in neutral fraction. Gaussian regions of lower emission correspond to regions of lower density, but H II regions usually have higher than average density and a dramatically lowered neutral fraction. This can be used for distinguishing Gaussian fluctuations from those caused by the ionization from quasars in the simulation, but in real observations we will have to rely on the intrinsic properties of spectral dips to separate H II regions from density fluctuations. In the next two sections we will use our simulation to predict how such a separation can be made from the observational data.

4. Analysis of Simulated Lines of Sight

We now discuss how we use the output at consecutive timesteps from the simulation described in §2 to create synthetic spectra of redshifted 21 cm emission. These spectra reflect the large-scale distribution of gas density, spin temperature, and hydrogen neutral fraction. The spin temperature is computed self-consistently in the simulation including the effects of Ly-α pumping and collisions with electrons and neutral atoms (see Gnedin & Shaver 2004 for details). The pixel size in the spectra is set by the cell size of $2h^{-1}$ Mpc, which corresponds to a frequency range of about 0.2 MHz at $z \sim 9$.

The synthetic spectra are created by casting a random line of sight through the simulation box. Our simulated lines of sight span a significant fraction of the horizon distance, so we simulate the line of sight on a fixed past light-cone instead of a fixed cosmic time, using consecutive output files at different timesteps of the simulation. We also account for a finite observing beamsize by convolving the 21cm signal over a plane perpendicular to the line of sight with a Gaussian beam, with a physical radius that varies over the line of sight according to a fixed angular size of a radio beam Θ_b.

The starting redshift of our spectra is $z = 13$, which corresponds to a frequency of 101 MHz. This redshift was chosen to place the resulting frequency in the range of next-generation radio observatories. We used 450 independent lines of sight to accumulate sufficient statistics.

After the synthetic spectra were created in this way, we analyzed the brightness temperature distribution for signatures of H II regions. The process we followed for this analysis consists of the following steps. First, we fit the mean signal $\langle T_B \rangle$ with a fourth-degree polynomial in order to remove variations on a very wide frequency scale. This process, similar to the continuum fitting used in the analysis of Ly-α forest spectra, is intended as an approximation to the removal of the combined galactic and extragalactic foregrounds and the cosmological mean signal in an observation. Next, we calculate the fluctuating signal as:

$$\Delta T_B = T_B - \langle T_B \rangle, \tag{1}$$

to obtain a fluctuating signal with zero mean that can be searched for H II region dips. For the analysis we disregard all parts of the spectrum in which the emission exceeds the mean signal, which correspond to regions of high gas density that are part of linear Gaussian fluctuations. We are then left with a spectrum showing dips due to both Gaussian fluctuations (corresponding to regions of low gas density) and H II regions around bright sources (corresponding to regions of very low neutral fraction compared to the average medium).

5. Results

In Figure 2 we show an example of a typical line of sight with the mean signal subtracted. The top panel shows the brightness temperature fluctuation ΔT_B versus ν after subtracting the mean signal. A significant fluctuation due to an H II region

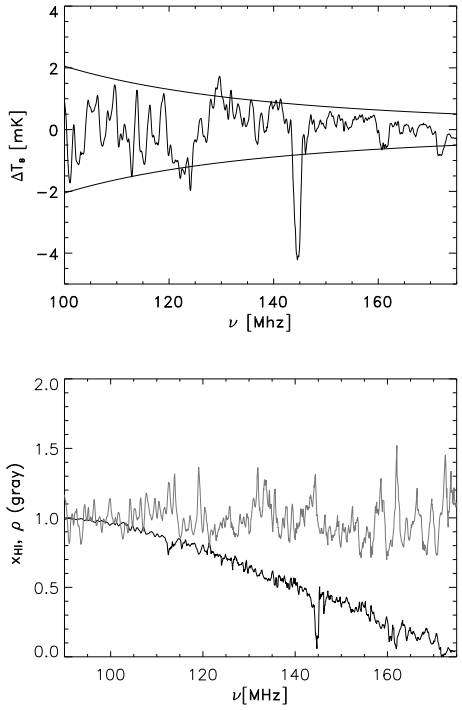

Fig. 2.— Top panel: the fluctuation in the brightness temperature ΔT_B as a function of frequency in a $10'$ beam with a 0.5 MHz bandwidth. Also shown are the 5σ sensitivity limits for a 1000 hrs integration time (Shaver et al. 1999). Bottom panel: the distribution of gas density (gray) and hydrogen neutral fraction (black) along the same line of sight. The H II region spectral feature can be seen at $\nu = 144$ MHz.

at $\nu = 144$ MHz is easily identifiable in the spectrum. Superimposed are the 5σ sensitivity limits for an integration time of 1000 hrs and a bandwidth of 0.5 MHz (we discuss our choice for the bandwidth below).

It is important to note here that our results differ to a small degree from the predictions of Tozzi et al. (2000) and Wyithe & Loeb (2004) in that we do not observe an increase in the redshifted 21 cm emission just outside the H II region. This is due to the fact that the main source of Ly-α radiation that couples the gas kinetic temperature and the spin temperature of the 21 cm transition in our simulation is normal galaxies. Since,in our simulation, galaxies typically form before the quasars, an

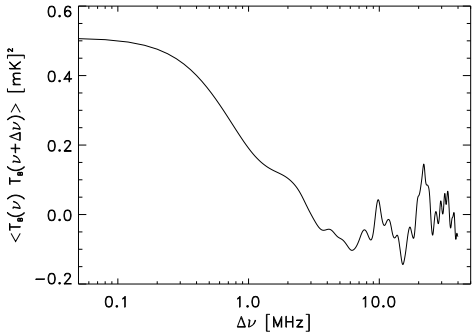

Fig. 3.— The auto-correlation function of the brightness temperature ΔT_B as a function of FWHM frequency width $\delta\nu$.

H II region around a typical high-redshift quasar expands in the already pre-heated gas, in which the spin temperature of the 21 cm transition is already much higher than the CMB temperature, so the extra Ly-α radiation from the quasar does not lead to an increase in the emission. We would like to re-emphasize here that, since we are treating the radiative transfer in full 3D, we do include the proximity effect of the increased Ly-α radiation around quasars, but this effect, as our results indicate, is not significant.

To distinguish H II regions from under-dense regions with low neutral hydrogen density, we now look at the distribution of density and neutral fraction in the same frequency range in the data obtained from the simulation.

The bottom panel in Figure 2 depicts the variations in these two parameters. The neutral fraction shows a dip at $\nu = 144$ MHz, whereas the density shows a definite increase. Consequently we can determine that this fluctuation results from a high density region containing more ionized gas than the average. We expect to find quasars in high density regions since their population is biased. If the radiation intensity were approximately uniform, we would expect to find lower densities of neutral gas in under-dense regions of the IGM, because of the decreased recombination rate. Here the high density and ionized fraction of the IGM allow us to conclude that the spectral dip is caused by an H II region surrounding a bright quasar.

The fluctuations in the brightness temperature on large scales are expected to be Gaussian, re-

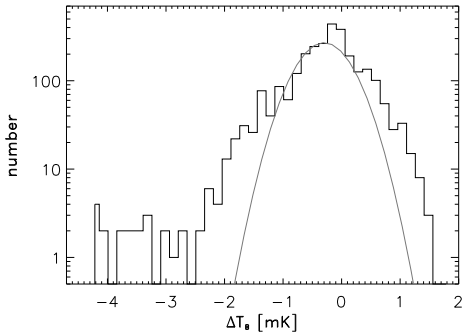

Fig. 4.— The histogram of ΔT_B for the normalized spectrum from Figure 2: notice the long tail of the non-Gaussian contribution from H II regions.

flecting the large-scale variations in the cosmic gas density and neutral fraction. However, on sufficiently small scales the fluctuations become correlated. Thus, unless the beam size of a radio telescope is small enough (less than about 1 arcmin) to resolve individual H II regions around high redshift galaxies, one would expect the cosmological signal to become smooth on scales comparable to the correlation length of high redshift galaxies. Figure 3 shows the auto-correlation length of the brightness temperature from the line of sight shown in Fig. 2 Thus, decreasing the bandwidth of observation to below about 0.5 MHz will not result in measuring new information in the signal unless it also coincides with a decrease in the beam size (this is also apparent from Fig. 11 of Gnedin & Shaver 2004). In the rest of this paper, we assume a fixed value of 0.5 MHz for the bandwidth for our fiducial beam size of $10'$.

In addition to investigating individual spectra as shown above, we can use the variations of brightness temperature around the average to look at the distribution of spectral dips statistically. Figure 4 shows a histogram of the difference in brightness temperature of the spectrum in Figure 2. One can see the tail of the distribution on the negative ΔT_B side that correspond to dips in the spectrum due to quasar H II regions. The peak centered around $\Delta T_B = 0$ is mainly due to the Gaussian fluctuations, but the long tail on the negative ΔT_B reaching $\Delta T_B = -4.5$ mK shows the significant contribution from regions that are due to ionized regions and not from Gaussian density

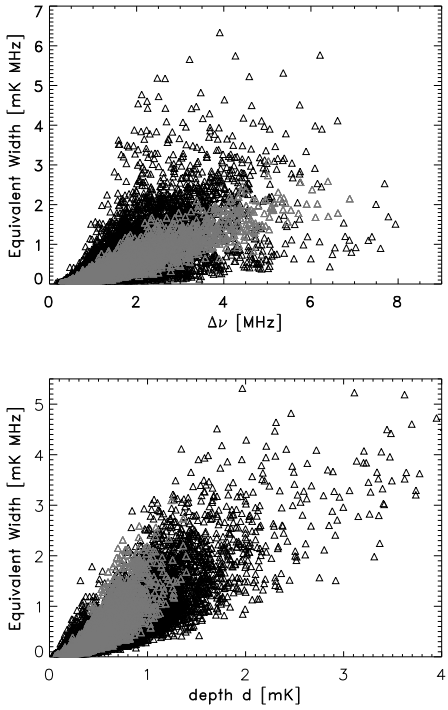

Fig. 5.— Top panel: in *black* is shown the distribution of equivalent widths and sizes of the spectral dips from 450 lines of sight. The *gray* data shows the same distribution for a pure Gaussian distribution. Bottom panel: A similar plot but for equivalent width versus the depth of the spectral dip distribution.

fluctuations.

We use a simple calculation of the equivalent width of each dip as a way to measure the dip depth. We integrate the area below the mean signal for each dip (i.e. a connected region with $\Delta T_B < 0$), and compile a distribution for all the dips of 450 different spectra. This distribution is shown in Figure 5 by plotting the equivalent width versus the dip width in frequency space (measured as FWHM). As a comparison, we also show the same distribution for artificial lines of sight that contain no H II regions, so that any dips are entirely due to Gaussian variations in cosmic density.

It is clear that the largest equivalent widths and depths correspond to H II regions around quasars, since the Gaussian density variations do not generate such large dips. The radial sizes, as shown

by $\Delta\nu$, of both samples are comparable, since the Gaussian density fluctuations also yield the wide dips seen in the spectra. However, the Gaussian fluctuations are much shallower, as can be seen by the smaller values in the equivalent width. There is also a range of smaller equivalent widths that is not reached with purely Gaussian fluctuations. This could be due to faint quasars in the simulation causing the small features. Judging from this graph, all spectral dips with equivalent width in excess of 3 mK MHz or depth in excess of 1.5 mK are caused by individual H II regions.

We can also look at cumulative distributions of various parameters characterizing these spectral dips, which are shown in Figures 6, to determine which are due to Gaussian fluctuations compared to the ones due to H II regions. The figure shows distributions for the simulated fluctuations in black and contrasts it with the distribution for pure Gaussian fluctuations in gray. From Figure 6a it is again clear that all spectral dips with equivalent widths in excess of about 3 mK MHz or depths in excess of about 1.5 mK are coming from high-redshift H II regions. The widths of the dips in frequency space, however, cannot be used to separate H II regions from linear Gaussian fluctuations. From these graphs we can infer that there is about a one in three chance to detect an H II region with equivalent width in excess of 3 mK MHz in each line of sight, but narrower deep dips (with depth in excess of 1.5 mK) are present in almost any line of sight.

The results shown in Figures 6 were obtained for a bandwidth of 0.5 MHz, but as long as the bandwidth is less than about 1 MHz, spectral dips from H II regions are resolved (as can be seen from Fig. 5a), and the distributions of equivalent widths and depths remain the same.

6. Discussion

We have shown that by far the easiest to observe features of the cosmological signal of redshifted 21 cm emission from neutral hydrogen in the pre-reionization era are the spectral dips due to individual H II regions from high-redshifts quasars. The largest of these features can be easily distinguished from Gaussian fluctuations due to large-scale structure: for example, we find that all spectral dips with equivalent width in excess of

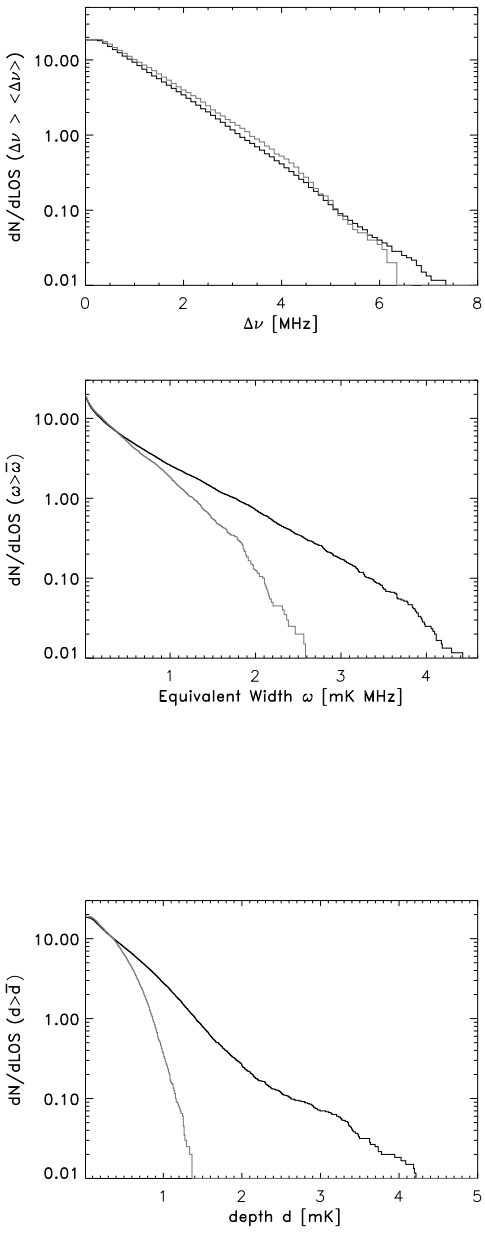

Fig. 6.— Top: The cumulative distribution of spectral dips per line of sight as the function of the dip width $\Delta\nu$ (measured as FWFM - *top*), the equivalent width (*middle*), and the depth (*bottom*) for the simulated spectra (*black*) and for purely Gaussian fluctuations (*gray*).

3 mK MHz or depth in excess of 1.5 mK come exclusively from quasar H II regions (for a 0.5 MHz bandwidth).

These dips are not rare - for our adopted plausible (albeit uncertain) extrapolation of the quasar luminosity function, detectable dips are present in almost every line of sight. This conclusion may sound counterintuitive to the common wisdom that "high redshift quasars are rare", but we need to emphasize that the quasars that create detectable H II regions are much less luminous (and much more numerous) than, say, SLOAN quasars. Besides, a $10'$ beam (for example) going from $z = 6$ to $z = 12$ (the onset of the FM radio band) contains a significant volume of about $500{,}000(h^{-1}\,\mathrm{Mpc})^3$. According to our model of the quasar luminosity function, there is about one quasar within this volume with blue rest-frame luminosity of $2 \times 10^{10} L_{Sun}$, and this luminosity is sufficient for a typical quasar to create an H II region that can be distinguished from Gaussian fluctuations due to large-scale structure. For a different model of the quasar luminosity function, our results can be simply scaled with the abundance of quasars above this characteristic luminosity.

Knowing the shapes and sizes of the ionized regions around quasars at high redshift could help to determine better the physical processes near super-massive black holes at the very first stages of structure formation in the universe. In particular, if observed spectral dips in the redshifted 21 cm emission can be identified with specific quasars observed in the infrared by, say, JWST, then a significant constraint can be placed on the lifetimes of quasars as a function of their luminosity. Such a constraint is difficult to obtain using other methods.

The depth distribution of spectral dips caused by H II regions can put a constraint on the residual neutral fraction inside H II regions. This neutral fraction would likely be locked in high-density, self-shielded gas clumps in collapsed halos (observed as Lyman limit systems in ultraviolet spectra), which play the dominant role for determining the clumping factor of ionized gas during reionization.

Under the assumption that the distribution of H II regions is statistically isotropic, it will be possible to put constraints on the residual neutral fraction inside H II region, and, since this neutral gas most likely is locked inside Lyman-limit systems, an important constraint can be put on the abundance of low mass objects.

In conclusion, the spectral features predicted in this paper - the spectral dips due to H II regions around individual high-redshifts quasars - will be the most prominent signals in the redshifted 21 cm line of neutral hydrogen from the pre-reionization era. Their spectral sharpness will easily distinguish them from the smoothly varying continuum spectra of the foreground emissions, and their strength should make them detectable in reasonable integration times with the new generation of low frequency radio telescopes.

REFERENCES

Chen, X., & Miralda-Escudé, J., 2004, ApJ, 602, 1

Cristiani, S., et al. 2004, ApJ, 600, L119

Di Matteo, T., Perna, R., Abel, T., & Rees, M. J. 2002, ApJ, 564, 676

Fan, X., at al. 2003, AJ, 125, 1649

Gnedin, N. Y. 2004, ApJ, 610, 9

Gnedin, N. Y., & Shaver, P. A. 2004, ApJ, 608, 611

Gnedin, N. Y., Abel, T. 2001, NA, 6, 7, 437

He, P., Liu, J. , Feng, L. , Bi, H., & Fang, L. 2004, ApJ, 614, 6

Kohler, K., Gnedin, N. Y., & Miralda-Escudé, J. 2004, in preparation

Loeb, A., & Zaldarriaga, M. 2004, PhRevL, 92, 211301

Madau, P., Meiksin, A., & Rees, M. J. 1997, ApJ, 475, 429

Oh, P. S., & Mack, K. J. 2004, MNRAS, 346, 871

Santos, M. G., Cooray, A., Haiman, Z., Knox, L., & Ma, C. 2003, ApJ, 589, 756

Scott, D., & Rees, M. J. 1990, MNRAS, 247, 510

Shapiro, P. R., Iliev, I. T., & Raga, A. C. 2004, MNRAS, 384, 753

Shaver, P.A., Windhorst, R. A., Madau, P., & de Bruyn, A.G. 1999, Å, 345, 380-390

Schirber, M., & Bullock, J. S. 2003, ApJS, 584, 110

Tozzi, P., Madau, P., Meiksin, A., & Rees, M. J. 2000, ApJ, 528, 597

Wyithe, J. S. B., & Loeb, A. 2004, ApJ, 610, 117

Zaldarriaga, M., Furnaletto, S. R., & Hernquist, L. 2004, ApJ, 608, 622

This 2-column preprint was prepared with the AAS LaTeX macros v5.2.